Time-Resolved High Speed Visualization and Analysis of Underwater Shock Wave Focusing Generated by a Magnetic Pulse Compression Unit

D. Oshita, S.H.R. Hosseini, *Member, IEEE,* Y. Okuda, Y. Miyamoto, T. Sakugawa, *Member, IEEE,* S. Katsuki, *Member, IEEE,* H. Akiyama, *Fellow, IEEE*

***Abstract*—Paper reports on visualization and analysis of underwater shock waves generation, focusing, and propagation. Recently, shock waves have been attractive with rising attention in medical field. Extracorporeal shock wave lithotripter (ESWL) has been one of its very successful applications. However, the effects of shock waves on living tissue are not sufficiently understood, due to unknown parameters involving the shock wave interaction. For better understanding of affecting points, a precise and controllable shock wave source is required. In this paper, in order to study shock wave effects, pulsed electric discharges produced by magnetic pulse compression circuit (MPC) were used to generate underwater shock waves. A half-ellipsoidal reflector was used for shock wave focusing. The whole sequences of the shock wave generation, propagation, focusing and cavitation bubbles, which appeared after shock wave passage, were visualized by time-resolved high speed shadowgraph method. The peak pressure of shock wave focusing at 2nd focal point reached 180 MPa. A cylindrical test section was used to observe phenomena around the electrode from the pulse discharge to bubble collapse. The first cavitation bubble's collapse occurred at about 750 μs. In the experiment, the two shock waves, one generated by expansion of plasma and another generated by collapse of the cavitation bubble were studied. Using high speed visualization and image analysis, the velocity and pressure of the two shock waves were evaluated. The peak pressure of shock wave generated by bubble collapse reached 157 MPa.**

***Index Terms*—Underwater shock wave, magnetic pulse compression circuit, high speed visualization, cavitation bubble, medical application**

I. Introduction

Shock waves have been studied for their various scientific and industrial applications. In medical field, shock waves have been successfully applied. In extracorporeal shock wave therapy (ESWT), shock waves are produced outside the body and are acoustically coupled with the skin, and then propagate in tissue to focus on a targeted area for treatment [1]. This process for the stone fragmentation in medicine is well known as extracorporeal shock wave lithotripsy (ESWL), which has been the most successful medical application of shock waves.

Shock waves have been a common practice for treatment of urinary stones for more than two decades [2]. Recently, applications of underwater shock waves have been extended to various clinical therapies [3], e.g., in orthopedic surgery for bone formation [4], for cancer therapy and enhancement of chemotherapeutic effects [5] [6], for revascularization of cerebral thrombosis [7] [8], and for drug delivery [9] [10]. The first medical application of micro-explosion for direct blasting of bladder stones was carried out by Watanabe and Oinuma [11]. Micro-explosive and double exposure holographic interferometric visualization have been used for extracorporeal shock wave studies [12] [13].

In the present research a compact shock wave generator has been designed and studied to produce micro shock wave focusing. In order to produce a range of underwater shock waves, micro-electric-discharge in electrolyte of degassed saline was used. A wide range of repeatable shock waves suitable for in-vivo and in-vitro medical applications was obtained.

The whole sequence of the shock wave generation, propagation, and focusing was visualized by using a time-resolved high speed shadowgraph method. Qualitative and quantitative data were obtained to study shock waves and the subsequent cavitation bubble generation for medical application. Cavitation around the electrode from just after the pulse discharge to bubble collapse was observed.

II. Experimental Method

Fig. 1 shows a schematic diagram of the experimental set up. High speed time-resolved shadowgraph method was used for the flow visualization. A magnetic pulse compression (MPC)

Manuscript received September 30, 2011; this work was supported in part by the Global Center of Excellence Program on Global Initiative Center for Pulsed Power Engineering from the Ministry of Education, Culture, Sports, Science and Technology, Japan.

D. Oshita, S.H.R. Hosseini, Y. Okuda, Y. Miyamoto, T. Sakugawa, S. Katsuki and H. Akiyama are with the Graduate School of Science and Technology, Kumamoto University, Kumamoto 860-8555, Japan.

S. H. R. Hosseini, S. Katsuki, and H. Akiyama are also with the Bioelectrics Research Center, Kumamoto University, Kumamoto 860-8555, Japan.

(Corresponding e-mail: hosseini@kumamoto-u.ac.jp).

circuit developed in our group [14], a digital scope (Tektronix DPO4104, USA), a high speed camera (ULTRA Cam HS-106E, Nac Company, Japan), and a flash lamp were connected with a delay unit (Stanford Research System Inc., Model DG535, USA) to adjust the timing. The MPC setting typically used in the experiments had peak output voltage and current up to 20 kV and 1.2 kA, pulse width of 200 ns (FWHM), and impedance of 100 Ω. The load resistant was matched with the MPC to prevent the circuit from ringing. Current and voltage were measured by a current monitor (Pearson, Model 5046, USA) and a high voltage probe (Tektronix P6015A, USA), respectively. The shock wave pressure was measured by a fiber optic probe hydrophone (FOPH 2000, RP acoustics, Germany). Fig. 2 shows the photograph of experimental outline.

Two types of experiments were performed. A half-ellipsoidal geometry was used for shock wave focusing. A cylindrical test section was used to observe bubble growth around the electrode from the pulse discharge to bubble collapse. The half-ellipsoidal reflector with 20 mm opening diameter was constructed as an extracorporeal shock wave source. Fig. 3 shows a schematic diagram of the reflector. The shock wave reflector was made of brass. Cylindrical tungsten with 0.9 mm diameter was used as electrode. The gap distance of electrode in the reflector was fixed between 0.2 mm to 0.4 mm. Spherical shock waves were generated by the electric discharge. The water was degassed by a vacuum pump in order to eliminate the influence of dissolved air.

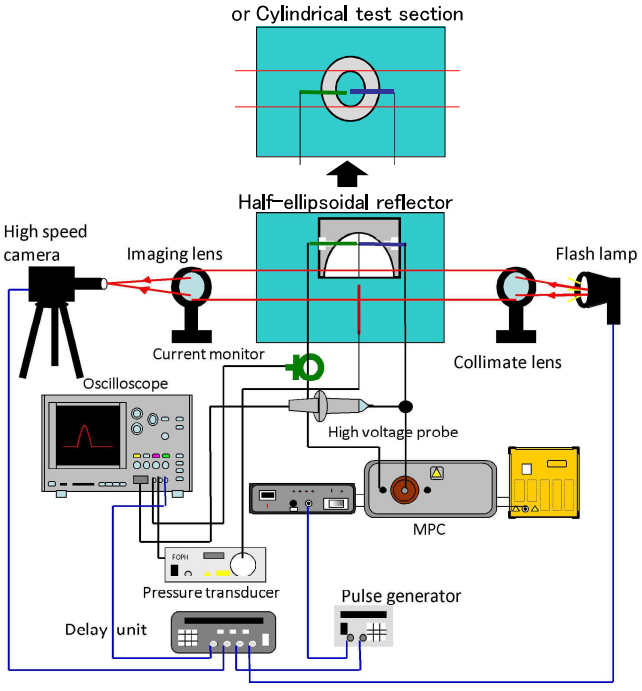

Fig. 1. Schematic diagram of experimental optical setup for shock wave visualization using high speed camera. A half-ellipsoidal reflector was used for shock wave focusing. The reflector was replaced with a cylindrical test section to observe the bubble growth around the electrode from the pulse discharge to the bubble collapse.

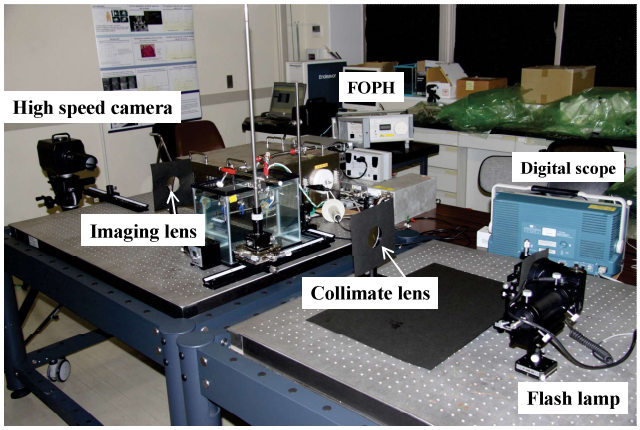

Fig. 2. The photograph of the experimental apparatus outline.

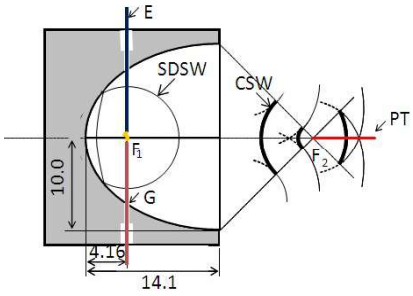

Fig. 3. Schematic diagram of a half-ellipsoidal shock wave reflector (E: electrode; G: ground; SDSW: spherical diverging shock wave; CSW: converging shock wave; PT: pressure transducer; F_1: 1st focal point; F_2: 2nd focal point).

III. Experimental Results

A. Focusing Shock Wave

Fig. 4 shows selected images of time-resolved shadowgraph visualization of shock wave focusing recorded with 1 μs inter-frame time (1 million frames per second recording speed) and 100 ns exposure time. In each experiment 120 images were recorded. At 8 μs after the discharge, a spherical shock wave emerged out of the generator. A solid line visible from right to the 2nd focal point is the optical fiber pressure transducer, marked as PT in Fig. 4. At 10 μs, the diverging shock wave before arriving to the optical fiber probe and the reflected shock wave form the reflector's exit edge were well visualized. At 11 μs, the reflected shock wave from the reflector's wall converged toward the 2nd focal zone. At 18 μs, the focusing shock wave approached the 2nd focus. At 19 and 20 μs, the shock wave in focal zone traversed the optical fiber probe hydrophone pressure transducer. At 20 μs, cavitation appeared behind the focusing shock wave. Fig. 5 shows the focal area after the complete passage of shock wave, where considerable amount of cavitation bubbles were observed. The voltage and current waveforms of the electric discharge are shown in Fig. 6. In Fig. 6 the plot with open squares shows the voltage and line with filled diamonds shows the current. Fig. 7 shows the pressure at

the 2nd focal point. As can be seen from Fig. 7, the pressure had a negative part which was considered as a main factor to produce cavitation. The peak pressure reached 180 MPa and was high enough to effectively disintegrate kidney stone. The spherical diverging shock wave (SDSW) had over-pressure of 10 MPa, while it was 180 MPa for the focusing shock wave (SWF). The peak pressure was gained 18 times by the shock wave focusing.

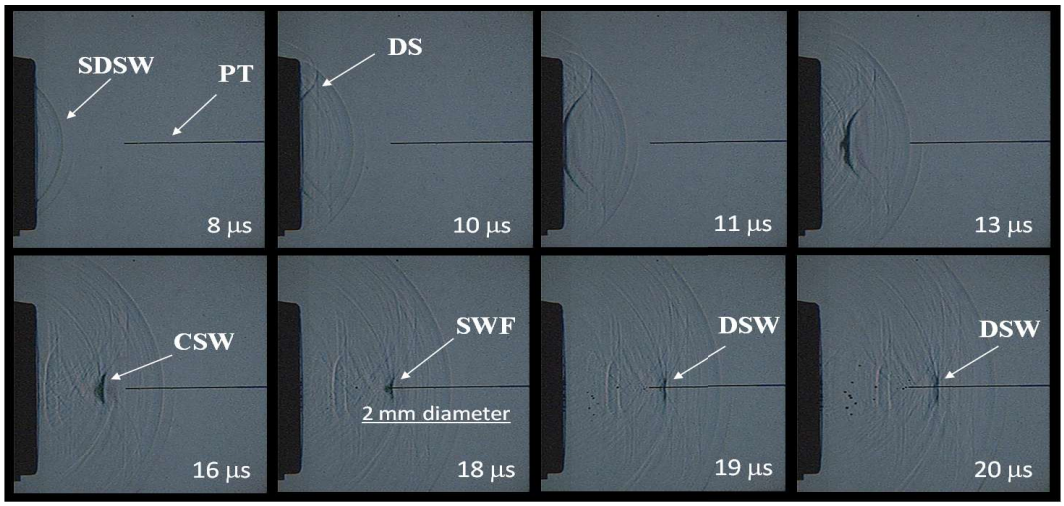

Fig. 4. Framing shadowgraphs for shock wave focusing (SDSW: Spherical Diverging Shock Wave; DS: Diverging Shock Wave; CSW: Converging Shock Wave; SWF: Shock Wave Focusing; DSW: Diverging Shock Wave after focusing).

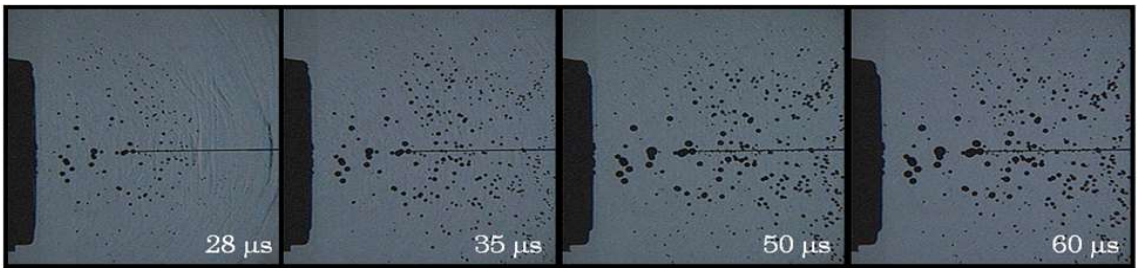

Fig. 5. Framing shadowgraphs of cavitation (after complete shock wave passage).

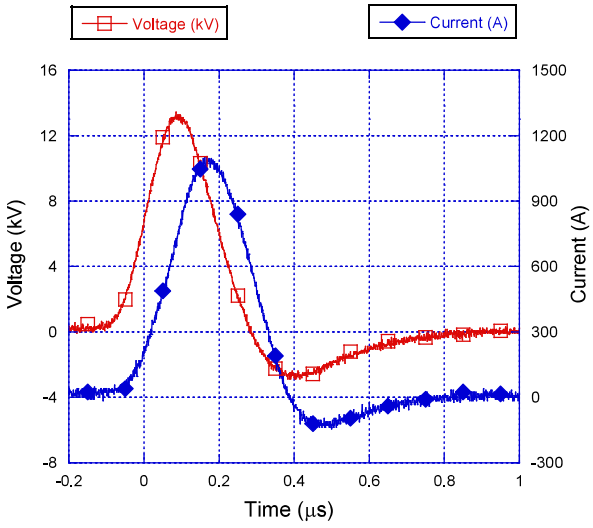

Fig. 6. Voltage and current waveforms.

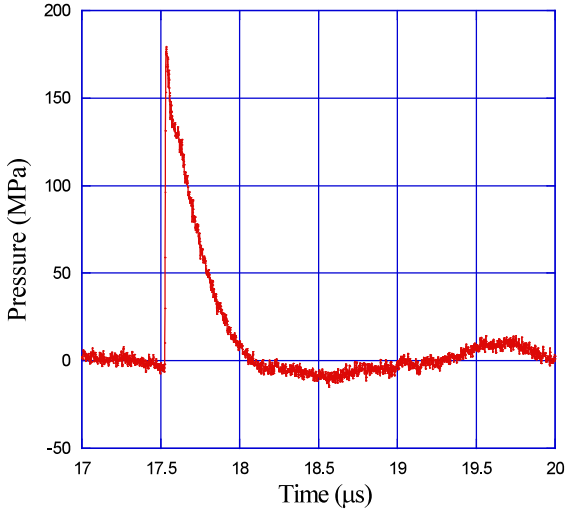

Fig. 7. Pressure histories measured by FOPH at the 2nd focal point.

B. Bubble growth from discharge to collapse

A cylindrical test section was used to observe bubble growth around the electrode from just after the pulse discharge to bubble collapse. The cylindrical test section permitted direct visualization of shock wave generation, which could not be performed with the shock wave focusing reflector. Two types of shock wave were observed. First shock wave generated by expansion of plasma and another shock wave by collapse of bubble. Fig. 8 shows framing shadowgraphs from the discharge to bubble collapse. At 8 μs, the shock wave generated by plasma expansion is shown. After shock wave propagation, the bubble appeared and expanded up to 410 μs after the discharge. Following the expansion, the bubble shrank and then collapsed, generating a secondary shock wave (Fig. 8, frames at 690 μs and 750 μs). After the first collapse, the bubble appeared again and collapsed with lower energy (Fig. 8, frame at 790 μs). Analysis of the two types of shock wave is performed in the next section. Fig. 9 shows histories of the bubble radius and the bubble velocity which was obtained and calculated from time resolved visualization experimental data. As can be seen in Figs. 8 and 9, the bubble collapse took place at about 750 μs. The high frame number of time-resolved high speed was very helpful to capture the bubble behavior near the electrode.

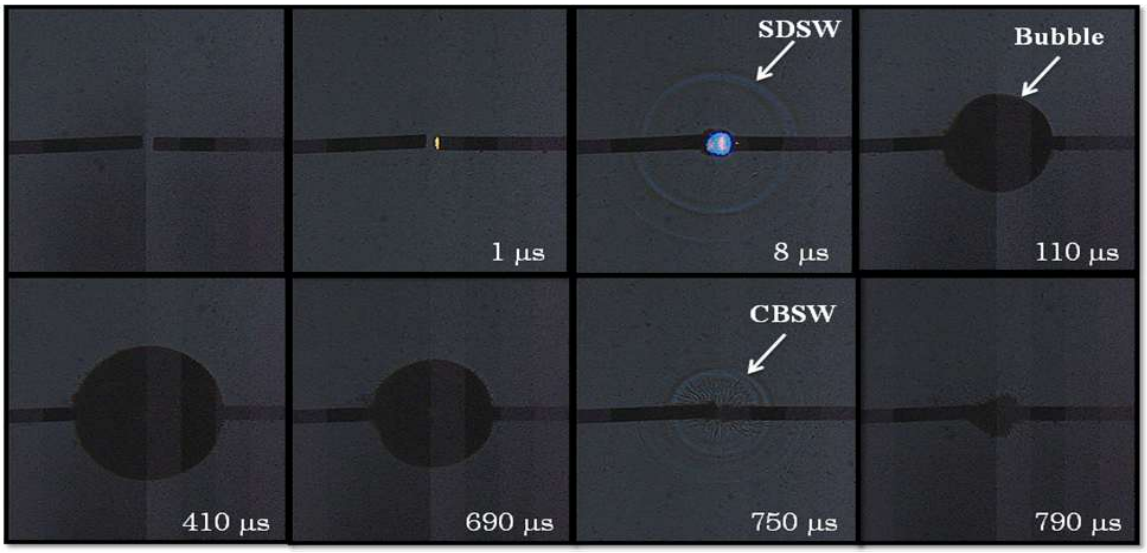

Fig. 8. Framing shadowgraphs of underwater discharge, shock wave generation, growth of bubble, bubble collapse, and secondary shock wave generation (SDSW: Spherical Diverging Shock Wave; CBSW: Collapse bubble generates shock wave).

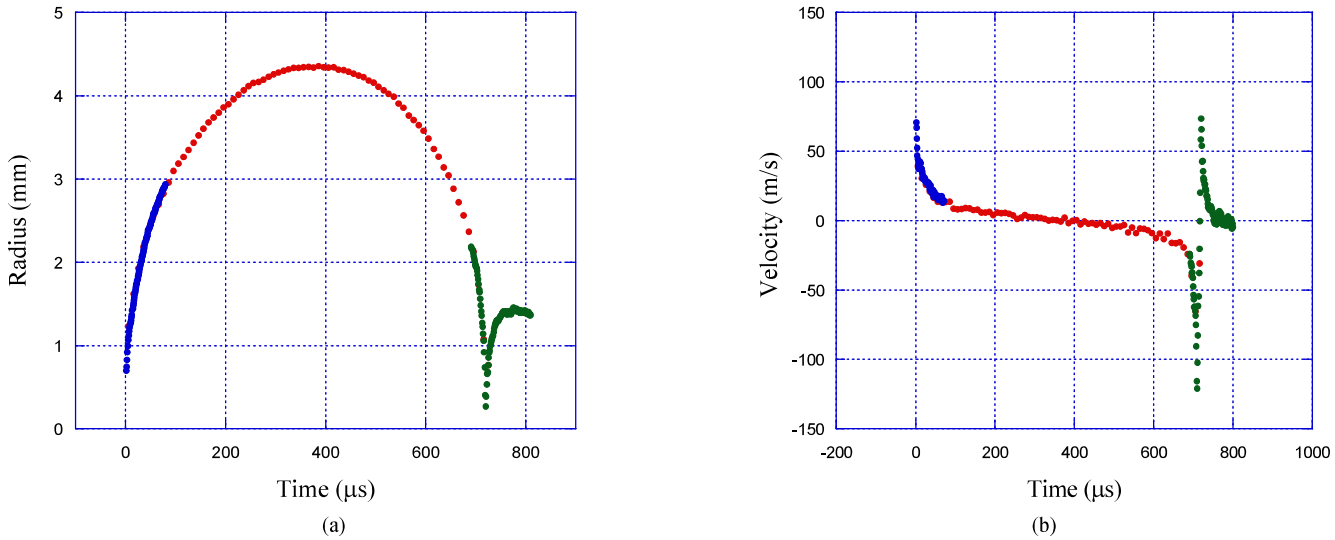

Fig. 9. Time variation of (a) bubble radius; and (b) bubble velocity. The data are from three visualization experiments which were done with the same initial conditions and parameters except for the frame rate and timing of the high speed camera to capture the bubble near the collapse.

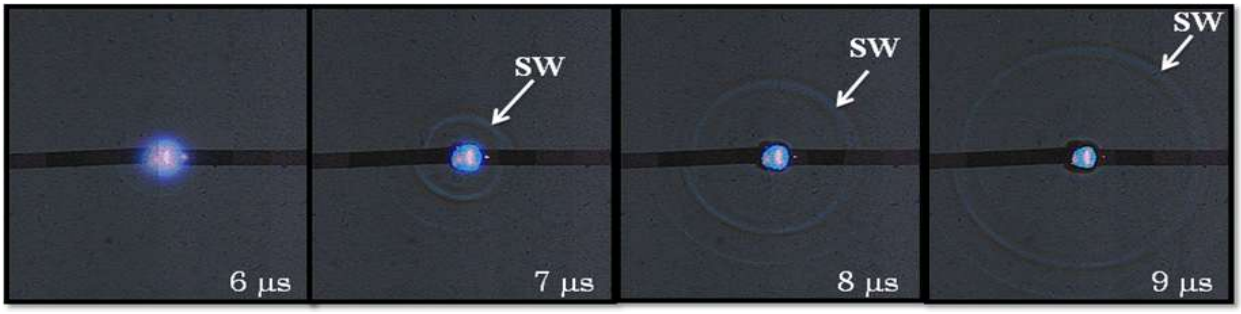

Fig. 10. Framing shadowgraphs of the first shock wave generated by plasma expansion (SW: Shock Wave).

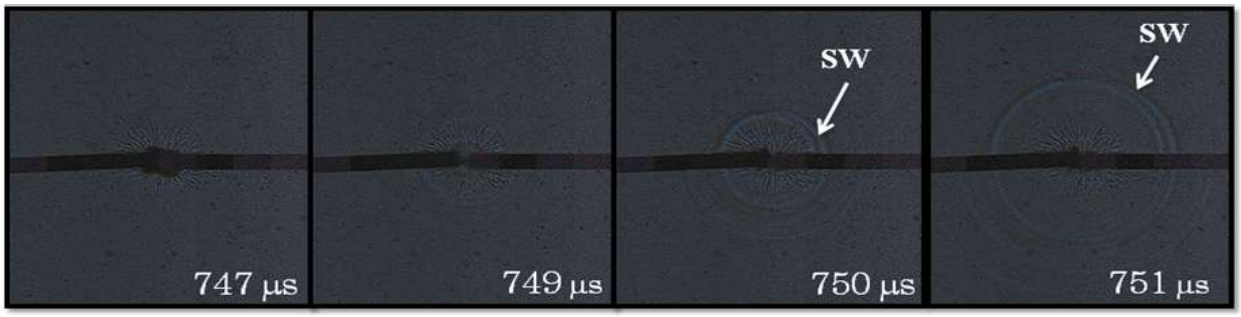

Fig. 11. Framing shadowgraphs of the secondary shock wave generated by bubble collapse (SW: Shock Wave).

C. Analysis of first and secondary shock waves

Fig. 10 shows framing shadowgraphs from the discharge to shock wave generation and propagation. The plasma expansion drove the spherical shock wave in water. In the second frame of Fig. 10, at 7 μs, the separated shock wave from plasma was well recognized; subsequently the shock wave diverged and became weak by propagation.

Fig. 11 shows framing shadowgraphs of the bubble collapse with a secondary shock wave emission. After 748 μs from the discharge, the convergence of the bubble energy with the bubble collapse took place, which generated the secondary diverging shock wave. The propagation of the secondary shock wave is shown in Fig. 11.

Fig. 12 shows time variation of shock wave velocities generated by the discharge and the bubble collapse. As can be seen in Fig. 12, the peak velocity of shock wave generated by the plasma expansion is approximately 1.83 km/s whereas the peak velocity of bubble collapse shock wave is about 1.75 km/s.

Fig. 13 shows time variation of shock wave pressure, which was calculated from Rankine-Hugoniot relations of saline electrolyte [15] using the shock wave velocity data of Fig. 12. The peak pressure of shock wave generated by the plasma expansion reached 250 MPa at about 3 mm from the electrode whereas the peak pressure of bubble collapse shock wave was 157 MPa. Both pressures rapidly decreased by the shock wave divergence. It should be noticed that due to the intense light production after the discharge, the direct measurement of pressure near the electrode was not possible. The intense light of the plasma interfered with the laser light of the FOPH and overloaded the FOPH for several microseconds.

Although the peak pressure of shock wave generated by the bubble collapse was weaker than the one produced by plasma expansion, 157 MPa is considerably high and is enough to produce secondary shock wave focusing. This would be

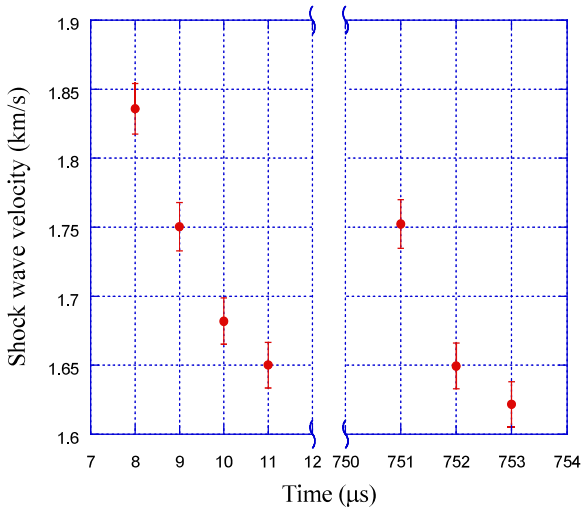

Fig. 12. Time variation of shock waves velocities; data of 8 μs to 11 μs are from the shock wave generated by plasma expansion and data of 751 μs to 753 μs are from the secondary shock wave produced by the bubble collapse.

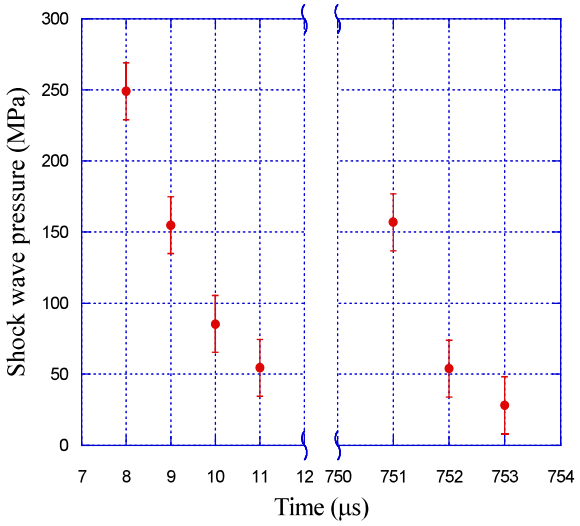

Fig. 15. Histories of shock wave pressure(at 8 μs to 11 μs are shock wave generated by plasma expansion and at 751 μs to 753 μs are shock wave generated by bubble collapse.)

valuable for controlling the cavitation bubble to produce a tailored secondary shock wave focusing and use its benefits in medical applications, such as cancer therapy.

IV. Summary and Prospect

Micro-electric discharges were used to generate spherical underwater shock waves. The reflected shock wave was employed to produce converging shock wave and generate strong shock wave at focus with up to 180 MPa pressure. The shock wave generator has appropriate shock energy for therapeutic applications, like shock wave bone formation or cancer therapy.

The whole sequence of shock wave generation by discharge plasma, bubble growth, bubble collapse, and secondary shock wave generation near the electrode were observed in a cylindrical geometry. The first bubble collapse took place at 750 μs, then it experienced secondary growth with dissipated energy and secondary collapse with much less energy and this process continued up to approximately 1.5 ms. By analyzing the flow visualization data and employing Rankine-Hugoniot relations, the shock waves velocities and pressures were evaluated. The peak pressure of shock wave generated by the plasma expansion reached 250 MPa at 3 mm of the electrode; then decreased rapidly with propagation. The bubble collapse shock wave had a peak pressure of 157 MPa. The considerably strong secondary shock wave would be beneficial for medical application. Visualization of shock wave focusing produced by secondary bubble collapse shock wave would be subject of our future paper.

References

[1] S.H.R. Hosseini, V. Menezes, S. Moosavi-Nejad, T. Ohki, A. Nakagawa, T. Toiminaga, K. Takayama, Development of shock wave assisted therapeutic devices and establishment of shock wave therapy, Minimally Invasive Therapy, 15, 230-240 (2006).

[2] M. Delius, Lithotripsy, Ultrasound in Med. Biol., 26, Sup.1, S55-58 (2000).

[3] K. Takayama and T. Saito, Shock wave/geophysical and medical applications, Annu. Rev. Fluid Mech., 36, 347 (2004).

[4] K. Ikeda K, K. Tomita, K. Takayama, Application of extracorporeal shock wave on bone: Preliminary report, J. Trauma, 47,946 (1999).

[5] M. Kambe, N. Ioritani, S. Shirai, K. Kambe, M. Kuwahara, D. Arita, T. Funato, H. Shimadaira, M. Gamo, S. Orikasa, R. Kanamaru, Enhancement of chemotherapeutic effects with focused shock waves: Extracorporeal shock wave chemotherapy (ESWC), In Vivo, 10,369 (1996).

[6] S. Moosavi Nejad, S.H.R. Hosseini, M. Sato, K. Takayama, Shock wave induced cytoskeletal and morphological deformations in a human renal carcinoma cell line, Cancer Science, Vol. 97, pp. 296-304 (2006).

[7] S.H.R. Hosseini, T. Hirano, O. Onodera, K. Takayama, Study of Ho:YAG laser generated underwater shock waves and cavity bubble for revascularization therapy, Advances in Bioengineering, ed. T.A. Conway, ASME BED 48,171 (2000).

[8] T. Hirano, M. Komatsu, T. Saeki, H. Uenohara, A. Takahashi, K. Takayama, T. Yoshimoto, Laser Sur. Med. 29,360 (2001).

[9] M. Delius and G. Adams, Shock wave permeabilization with ribosome inactivating proteins: a new approach to tumor therapy, Cancer Research, 59,5227 (1999).

[10] M. Kendall, T. Mitchell, P. Wrighton-Smith, Intradermal ballistic delivery of micro-particles into excised human skin for pharmaceutical applications, J. Biomechanics, 37,1733 (2004).

[11] H. Watanabe and S. Oinuma, Studies on the application of microexplosion to medicine and biology. I. Development of special explosive for the experiments, Japanese Journal of Urology, 68,243 (1977).

[12] K. Takayama, Application of holographic interferometry to shock wave research, SPIE, 398:174 (1983).

[13] M. Kuwahara, K. Kambe, S. Kurosu, S. Kageyama, N. Ioritani, S. Orikasa, K. Takayama, Clinical application of extracorporeal shock wave lithotripsy using microexplosions, J. Urology, 137,837 (1987).

[14] M. Akiyama, T. Sakugawa, S.H.R. Hosseini, E. Shiraishi, T. Kiyan, H. Akiyama, High-Performance Pulsed-Power generator Controlled by FPGA, IEEE Trans. Plasma Sci., Vol. 38, pp. 2588-2592 (2010)

[15] A. B. Gojani, K. Ohtani, K. Takayama, S.H.R. Hosseini, Shock Hugoniot and equations of states of water, castor oil, and aqueous solutions of sodium chloride, sucrose and gelatin, Shock Waves, DOI 10.1007/s00193-009-0195-9, pp. 1-6 (2009)